LU:research

Combined flow cytometry and confocal laser scanning microscopy for evaluation of BR96 antibody cancer cell targeting and internalization

Amir H. Iranpour Feridani[1][*], Bo Holmqvist[2], Hans-Olov Sjögren[3], Sven-Erik Strand[4], Jan Tennvall[1], Bo Baldetorp[1]

[1]Department of Oncology, Lund University, Sweden
[2]Department of Pathology, Lund University, Sweden
[3]Department of Immunology, Lund University, Sweden
[4]Department of Medical Radiation Physics, Lund University, Sweden

email: Amir H. Iranpour Feridani (Amir.Iranpour@med.lu.se)

[*]Correspondence to Amir H. Iranpour Feridani, Department of Oncology, Lund University, Lund, S-221 85, Sweden

ABSTRACT

Background:
Monoclonal antibodies (mAb) are important tools in the management of tumor disease, and the discovery of antibodies with both specific cancer cell targeting and capacity to enter the cells by internalization are critical to improve the therapeutic efficacy.

Method:
Antibody cancer cell targeting and internalization properties of fluoroscein-conjugated mAb made against Lewis Y (BR96) were evaluated quantitatively and qualitatively by means of flow cytometry (FCM) and confocal laser scanning microscopy (CLSM), respectively, on cells from a rat tumor cell line (BN7005-H1D2).

Results:
The study demonstrated a specific binding of BR96 to LewisY (LeY) located in the cell membrane and as BR96/LeY immunocomplexes (BR96/LeY) internalized into the cytoplasm. BR96/LeY was internalized into about 15% of the cells, usually distributed throughout the cytoplasm, but also located close to the nuclei. Cytotoxic effects by BR96 were indicated, and CLSM visualized subpopulations containing cells with bound or internalized BR96/LeY that possessed morphologically pyknotic nuclei and disrupted DNA.

Conclusion:
The spatial-temporal pattern by BR96 cell targeting and internalization processes of BR96/LeY into the cancer cells expressing LeY was demonstrated by FCM and CLSM. Used together, the FCM and CLSM techniques provide a valuable tool for preclinical analyses of antibody targeting and their capacities as carriers of cytotoxic conjugates for the use in cancer therapy.

INTRODUCTION

The use of monoclonal antibodies (mAb) in cancer therapy offers great potential as a specific drug delivery system ([1][2]) and may act as carriers of toxins or cytostatic drugs for chemotherapy ([3-6]), or of radionuclides for radioimmunotherapy ([7][8]). To ensure optimal therapeutic effects with mAb-bound agents, the critical components are target specificity, homogeneous binding properties, and the capacity of mAb as carriers of anticancer agents. Furthermore, when using mAb conjugated to toxins and short-range-particle-emitting radionuclides, the capacity for mAb to enter into the cancer cells (internalization) is an imperative for tumor eradication. Therefore, investigative tools for preclinical evaluation of the properties of mAbs are critical in order to optimize the mAb-based therapy and to develop new mAb-conjugates against different types of cancers.

The mAb BR96 has been demonstrated to possess specificity to LeY and high recognition capacity of most adenocarcinomas, combined with low binding to normal cell types ([9]). In addition, BR96 has the capacity to enter cancer cells and is indicated to possess properties of being cytotoxic in itself via mediation of antibody-dependent cellular cytotoxicity and complement-dependent cytotoxicity ([9-12]). Despite these beneficial properties, the use of BR96 in cancer therapies has provided unclear results ([13-16]), which urged further preclinical analyses of its target specificity and internalization properties of cancer cell populations or whole tumors to be able to optimize its therapeutic use. BR96 comprises a chimeric humanized mouse IgG that targets the LeY antigen expressed by various cancer cells, localized in the cell plasma membrane ([17][18]). The internalization process, or endocytosis, of BR96 bound to LeY as an immune complex (BR96/LeY) has been demonstrated to involve the same clathrin-coated pits as the transferrin receptor ([10]). The internalized BR96/LeY fuses with endosomes that ultimately undergo lysosomal degradation ([3][10]). The degree of internalization may differ between cells within the same tumor, independently of the amount of receptor binding, thus leading to a mixture of high- and low-internalized subpopulations. This heterogeneity in internalization has significant effects on the therapeutic efficiency of the antibody-cytotoxic complex. Furthermore, evaluations of BR96 as a carrier of anticancer agents, such as toxins and low-energy-particle-emitting radionuclides, are desirable to improve its use in clinical practice.

Knowledge about the internalization processes of mAbs has mainly been obtained by indirect methods using radio-labeled surface antibodies or SDS page and Western blotting ([19][20]). Quantitative analyses using flow cytometry (FCM) allow fast evaluation of a large number of cells which provides statistically reliable data. FCM methods for detection of one fluorescence-conjugated mAb have previously been used to demonstrate binding and internalization ([21]). The so-called multicolor FCM enables analysis of differently labeled markers simultaneously in a high number of cells. Parts of the internalization process of the BR96/LeY have been revealed by means of analysis in situ at cellular and subcellular levels using CLSM and electron microscopy on a human breast cancer cell line (H3396) ([1][3][10-12][19-23]). Among the various cell imaging techniques available for analyses of tissues and cells labeled with fluorophores and/or antibody fluorescence conjugates, CLSM is commonly used to identify and visualize different specific components simultaneously at the cellular level ([24][25]). In combination with FCM, CLSM adds the abilities for qualitative analysis in situ of the sites for mAb binding and of putative internalization of mAb into the cells. In the present study, we therefore evaluated the use of three-color labeling of BR96, LeY, and cell nuclei for analyses with FCM and CLSM for investigations of the binding and internalization properties by BR96. Cancer cells from a rat colon tumor cell line BN7005-H1D2 ([19][26][27]) were used as targets.

MATERIALS AND METHODS

Cells and Cell Cultures

BN7005-H1D2 cells (H1D2) from a rat tumor cell line were cultured and incubated at 37°C in 10-ml flasks with 5 ml of medium, R10 (RPMI 1640 containing 10% fetal calf serum (FCS, preheated), (Sigma, Stockholm, Sweden) 1% sodium acetate (Sigma), 1% Hepes buffer (Sigma), and 0.1% gentamycin (Sigma)). Every 2-3 days, the cells were split by removing medium and washing the cells twice with 5 ml phosphate buffer saline (PBS, Sigma), followed by a wash with 1 ml trypsin ((Sigma) with 1 mM ethylene-diaminetetraacetic acid (EDTA)). Then 1.5 ml trypsin was added and the cell culture was incubated for 5 min at 37°C. Subsequently, the trypsin was removed with minimal cell loss, and the cells were reincubated for 4 min at 37°C. Detached cells were resuspended in 4 ml R10; a fraction of the solution was then added to a 10-ml flask containing 5 ml fresh R10 medium, and the cells were incubated at 37°C for 24 h.

Antibodies and Reagents

The following reagents for detection and visualization were used for the analyses with FCM and/or CLSM: BR96 mAb (kindly provided by Prof. P. Senter, Seattle Genetic, Seattle, WA) conjugated with FITC (BR96-FITC, Sigma) was used for detection of LeY binding by both FCM and CLSM; anti-human mouse-IgG, conjugated with biotin (anti-IgG, BD Pharmingen, San Diego, CA) was used for detection of BR96; streptavidin (BD Pharmingen) conjugated with phycoerythrin (PE for FCM) or with Texas red (TR, for CLSM) for binding to biotin; propidium iodide (PI, Sigma) was used for analysis of cell cycle phases with FCM; PI and ToPro3 (Invitrogen, Molecular probes, CA) were used as nuclear markers for analysis with wide-field epi-fluorescence or CLSM. 7-aminoactinomycin-D (7AAD ([28]), BD Pharmingen, for FCM) and the TUNEL cell death detection kit (TR conjugated, Roche, Mannheim, Germany, for CLSM) were used for detection of DNA content of damaged or dead cells.

Summarized Description of Study Design

The same sample groups were used for determination of cellular binding of BR96 and internalization of BR96 bound to LeY for analyses with both FCM and CLSM, including a few alterations in the end of the protocol (see details below). The degree of binding and internalization by BR96-FITC at temperatures of 4°C and 37°C were analyzed. Two cell samples of the H1D2 cell line were incubated with BR96-FITC at 4°C for 30 min prior to internalization. The temperature of one of the samples was increased from 4 to 37°C (to initiate internalization) and then kept constant for predefined times (0, 1, 2, 4, or 24 h). Subsequent incubation with anti-IgG (i.e., against BR96) was performed, enabling determination of the fraction of cell-associated BR96-FITC remaining on the cell plasma membrane at the defined incubation periods. Thereafter, cells were incubated with streptavidin conjugated with PE (streptavidin-PE) or TR (streptavidin-TR), for binding a fluorescence marker on the biotin of the anti-IgG. In the FCM analyses, the intensity of the fluorescence from FITC and PE was compared with the values for cells incubated at 4°C, i.e., cells lacking internalization. Prior to FCM and CLSM, for an overview of the fluorescence labeling in the whole cell culture (of BR96-FITC and anti-IgG-TR or -PE labeling), samples were analyzed with an epi-fluorescence microscopy (Olympus AX 60) equipped with the appropriate filter sets (i.e., for FITC, PE/PI (TRITC) and TR excitation and emission spectra). Digital images were grabbed (Olympus DP70) separately from the individual spectral channels and merged via the overlay function (DP70 software). For detection of damaged

and/or dead cells, cells were subsequently incubated with 7AAD for analysis with FCM, or were labeled with the TUNEL procedure for analysis with CLSM. For CLSM analyses, a subsequent incubation of cells was undertaken with ToPro3, a nuclear labeling for detection of all cells in the sample with cell nuclei with pyknotic appearance.

Preparation of Cells

Two days prior to FCM analysis, the cells from the cell culture were detached and mixed with 4 ml of R10 medium and transferred to a 10-ml test-tube. Large cell aggregates were permitted to sediment to the bottom for 5 min. Three milliliters of the supernatant was then carefully transferred to another test-tube and carefully mixed. Cell numbers were counted using a Bürker chamber. About 4×106 cells were added to a 10-ml flask containing 5 ml R10 medium in which the cells were incubated at 37°C for 24 h.

Following incubation, the cell concentration was determined again and 10^5 cells were added to each well of a 96-well plate (with flat bottoms). R10 medium, 150-200 µl, was added to each well, and cells were then incubated at 37°C for 24 h. The medium was then removed from each well, and the cells were washed once with 100 µl PBS. Cells were then incubated in BR96-FITC solution (1/100, diluted in cold R10), for 30 min on ice (4°C) in the dark.

Cells were then washed with 100 µl PBS (to remove unbound BR96-FITC), and 150 µl preheated (37°C) R10 was added to each well. The plates were incubated at 37°C, for 0, 1, 2, 4, and 24 hours, the medium was removed, and the cells were washed once with 100 µl PBS. Cells were then washed once with trypsin solution, followed by incubation in 100 µl fresh trypsin solution for 10 min at 37°C. Thereafter, R10 containing FCS (100 µl) was added (to inhibit the trypsin activity). Cells were transferred to the first of two 96-well plates (with round bottoms). The plate was centrifuged for 1 min at 200g (~1,200 rpm), and the cells were washed with 100 µl primary medium (PBS containing 10 mmol EDTA and 1% bovine serum albumin (BSA)) to lower cell clustering. Thereafter, the cells were spun down and washed with 100 µl secondary medium (PBS containing 2 mmol EDTA and 1% BSA). The cells were transferred to the second 96-well plate (round bottoms) that was put on ice in a light-depleted box until all the cell samples had been incubated.

The cells were resuspended in 50 µl of the secondary medium containing anti-IgG (1/100) and were incubated on ice for 20 min. The cells were spun down and washed once with 100 µl of the secondary medium and were thereafter resuspended in 50 µl secondary medium containing streptavidin-PE (1/200) and incubated for 20 min on ice. Finally, the cells were spun down and washed once again and resuspended in 200 ml secondary medium containing 7AAD (1/200). The cells were analyzed with FCM or were prepared further for CLSM analysis (see below).

Analysis of Cell Cycle Phase Distribution with FCM

Separate cell cycle analysis was performed, i.e., of the fractions of cellular nuclei in G_0/G_1, S or G_2/M phases. The staining of nuclear DNA content and FCM analysis were performed as previously described ([29][30]). Briefly, about 10^6 cells were mixed with 1 ml PBS, and were washed once in PBS. Samples were incubated in "nuclear isolation medium" containing PI (50 µg/ml) in the dark for 5 min at room temperature. Samples were then kept at 4°C for at least 15 min prior to flow cytometric analysis. Up to 20,000 nuclei/sample were analyzed. Processor signals were digitized and sorted into frequency distributions (i.e., as DNA histograms) with a resolution of 256 units. The distribution of the cell cycle phases of the analyzed cell population was determined by applying ModFit LT 3.1 software (Verity

Software House, Topsham, ME) to the DNA histograms. The contributions of nuclear debris and aggregates were taken into consideration when evaluating the DNA histograms, as outlined by "Guidelines for DNA flow cytometry" (http://www.sfff.se).

FCM Equipment and Analysis

FCM analysis was performed on a FACSCalibur flow cytometer (Becton Dickinson Immunocytometry Systems, San Jose, CA) equipped with the Cell Quest PRO™ program, which was used for the acquisition and analysis of the fluorescence data. The optical filter configuration for the simultaneous analysis of FITC-, PE- and 7AAD- fluorescence was used according to the recommendation of the manufacturer.

All fluorophores used for FCM, that is PI, FITC, PE, and 7AAD, were excited by laser light from an argon ion laser tuned to 488 nm. For the DNA FCM cell cycle analysis, the PI fluorescence was filtered through a band pass filter (585 ± 42 nm) before collection in linear mode. In the multicolor measurements, the FITC fluorescence emission was separated from the fluorescence emitted by PE and 7AAD by a dichroic mirror (560 nm) and thereafter filtered with a 530 ± 30 nm band pass filter before collection in logarithmic mode. PE fluorescence emission was separated from 7AAD emission by a dichroic mirror (640 nm) and, before logarithmic collection, filtered with a band pass filter (585 ± 42). The emission from 7AAD was filtered with a long wave filter (670 nm) before collection in linear mode.

The standardization procedure for FCM analysis was performed according to the general guidelines (http://www.sfff.se). The sensitivity of all fluorescence channels measured were tested by standard plastic beds (Becton Dickinson) and for the DNA content analysis we used PI-stained chicken and trout red blood cells prepared in our laboratory according to descriptions by Vindelöv and coworkers ([31]). Moreover, to ensure a constant setting of sensitivity between the different experiments, intensity values for the FITC- and PE-fluorescence from prepared/incubated control cells were used for adjustments of the gain settings of the correlating channels.

Exclusion of nonrelevant counts was performed by a gate which was set in the combined dot-plot of the forward-, versus side-light scatter (FSC and SSC), and versus 7AAD fluorescence signals. Thus, only events from cohort and intact cells were collected. Exclusion of dead or dying cell counts was performed on all cell counts by 7AAD fluorescence exclusion and thus only events from live and intact cells (10,000) were analyzed. Gates were then set on the wanted population in the forward- and side-scatter (FSC and SSC) signals. The mean fluorescence intensity values for the heterogeneous cell populations were statistically extracted by the permanent regions, R1 and R2, as defined in the fluorescence dot-plot graphs in Figure 1.

To calculate the mean normalized value of BR96 internalization for the studied cell populations at incubation times of t = 0, 1, 2, and 4 h, the following ratio was calculated:

$$RATIO = \frac{(FITC/PE)(t)}{(FITC/PE)(0)}$$

The values of ratio FITC/PE were normalized to the value at time zero to allow comparison of the experiments. Each data point in the fluorescence intensity versus time experiments is the mean ± 1 SD obtained from five different experiments.
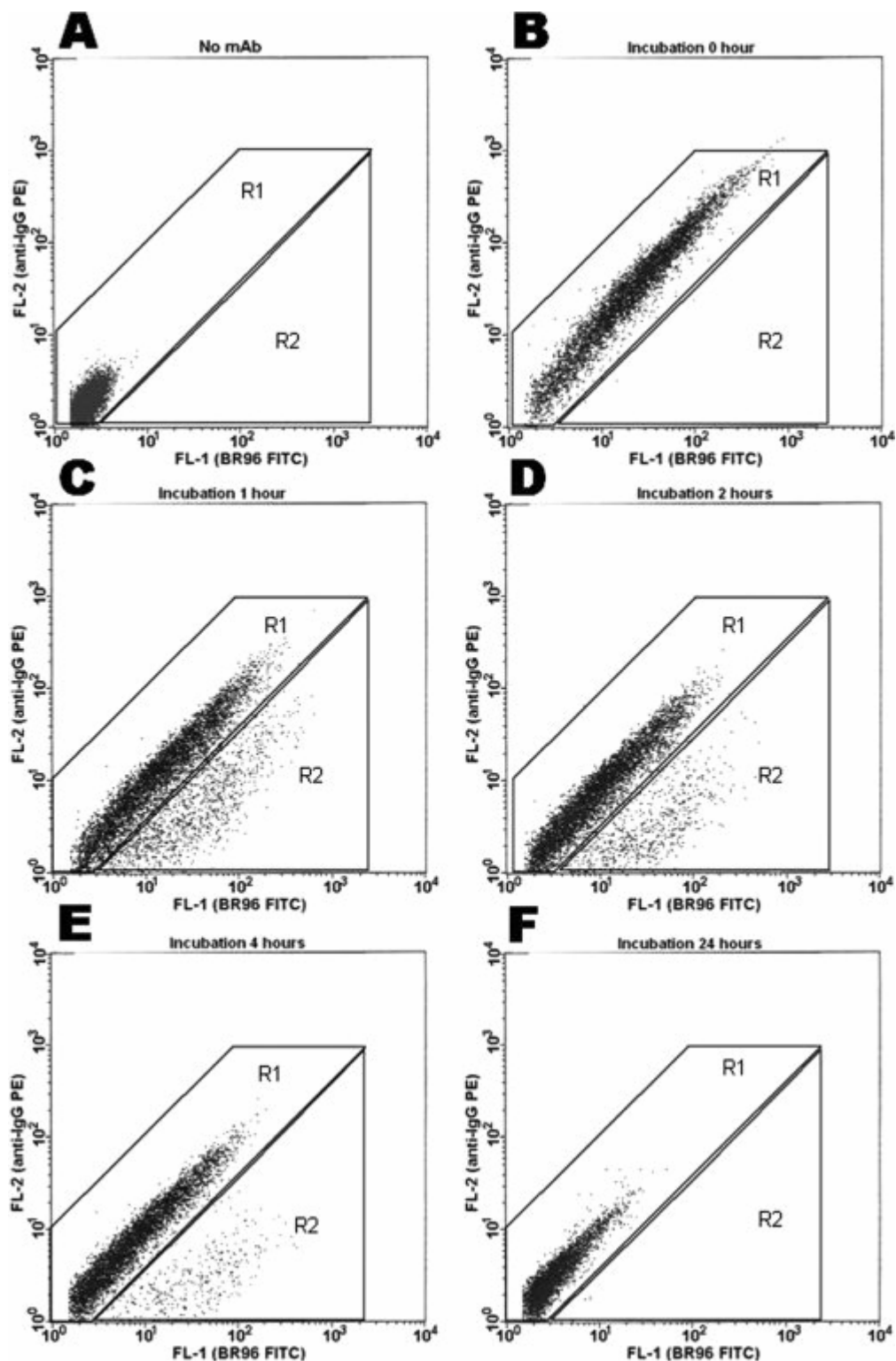
Figure 1.
Flow cytometric dot plot graphs from one experiment performed up to 24 h of incubation with FITC conjugated BR96 (A-F, see also Table 1). Each graph contains 10,000 collected and gated events. Abscissa versus ordinate: Logarithmic distributions of BR96-FITC versus anti-IgG-PE fluorescence signal per analysed cell. A: No mAbs were bound to the cells. B: BR96-FITC and anti-IgG-PE after zero hours of incubation. C-F: BR96-FITC and anti-IgG-PE after 1, 2, 4, and 24 h of incubation. The marked R2 area identifies a subpopulation of cells that shows the same BR96-FITC binding intensity but lower anti-IgG binding than the main population. This indicates that this population has been internalized by the BR96 FITC. Note that this population is not detected in B (at 0 hours of incubation). Also the subpopulation decreases with time as shown in the dot plots C-F.

CLSM Procedure

In the presented study, CLSM qualitative analyses was used solely for confirmation of the BR96 binding and internalization processes at the cellular (and subcellular) level, suggested by the statistical data obtained by quantitative FCM analysis. For CLSM, the cells were prepared as described above for FCM analysis. Between 150 and $1,000 \times 10^3$ cells were dispersed onto each object slide chamber, and R10 medium was added (250 µl to 2 ml depending on chamber size). Following incubation for 24 h at 37°C, the chambers were washed with PBS and the cells were incubated with BR96, in the dark for 30 min. After washes with PBS, slides were sampled (see below), or were continuously incubated for 1 or 2 h in R10 at 37°C. Sampled cells were rinsed with PBS and fixed in cold 4% para-formaldehyde (in PBS) for 5 min, followed by rinses in PBS 2×10 min. Cells were then incubated in biotin conjugated anti-human IgG antibodies (1:100) for 20 min (on ice). Following a rinse in PBS (5 min), cells were incubated in streptavidin-TR (for CLSM and wide-field epi-fluorescence microscopy) or streptavidin-PE (for wide-field epi-fluorescence microscopy; 1:100), for 20 min (on ice). Some cell chambers were incubated with TUNEL reagent for cell death detection (as described in manufacturers manual). Cells were then incubated with ToPro3 (1:1,000) for 30 min, after which rinses in PBS was performed (2×10 min). The chambers and the silicon layers (on the chambers) were removed and the cells were cover-slipped, mounted in PBS-glycerol containing p-phenylenediamine.

Initially, for an overview of the fluorescence labeling in the whole cell culture (of BR96-FITC and anti-IgG-TR or PE labeling), samples were analyzed with an epi-fluorescence microscopy (as described above). CLSM analysis was used for visualization of the cellular localization of BR96 binding sites, and its relation to the anti-IgG-TR of cellular structures (primarily localization at the plasma cell membrane and/or within the cytoplasm), and in relation to pyknotic ToPro3 labeled nuclei or TUNEL (TR) labeled cells. CLSM analyses were performed of representative regions of the cell cultures and subpopulations, from the different periods of BR96 incubation times (0, 1, and 2 h).

CLSM analysis was performed with a BioRad MRC 1024, controlled via LaserSharp (version 5.2 for PC/Windows) and mounted on an inverted Nikon microscope (Nikon Diaphot 300). For the analyses, we mainly used a Nikon 60× objective (PlanAPO 60/1.2, WI 160/0.16-0.18), with a maximum of two-times zoom function. A Krypton-argon laser was used (Dynamics Laser, Salt Lake city, UT), which is optimized for emission of signals at three wavelengths; 488 nm, 568 nm, and 647 nm, correlating with the detection of the photomultiplier tubes. The general CLSM operational variables were considered ([24][25]) in our study to obtain high resolution images with specific and optimal separation of individual signals. Settings were optimized for each fluorophore, and data acquisitions were obtained only by sequential (separate) scanning of individual fluorophores, which provided a total separation in the light collecting channels (i.e., of FITC, PE, TR, and ToPro3 fluorescence). The settings for laser intensity and PMT's for each channel were made via the "Set LUT" option, allowing settings with saturation of the strongest signals (such as the large aggregates of BR96 labeling) while retaining the relatively weaker signals of relatively lower intensity just above background. The same pinhole size was set for the channels visualizing FITC and TR. The level of auto-fluorescence recorded in all channels of nonincubated cell populations was used as a background signal, adjusted in the settings for the individual channels. The same settings were used when comparisons were made of the localization of labeling between the different treatments. Optical slices (around 300 nm) were collected in Z-steps through whole cells (up to 8 µm). The data, colocalization of BR96 and LeY, and their localization to the plasma cell membrane and/or within the cytoplasm were analyzed as individual optical sections, as merged images and as rotated 3D reconstructions (performed in Laser Sharp).

RESULTS

FCM Data

The cell cycle phases of H1D2 cells, obtained with DNA FCM, showed a G_0/G_1-phase fraction of 35%, S-phase fraction of 48% and a G_2/M-phase fraction of 17%. This corresponded to the obtained cell culture growth curves.

The results from FCM analyses are represented as dot-plots (Figs. 1A-1F). Dot-plots A-F demonstrate the logarithmic values of BR96-FITC versus anti-IgG-PE fluorescence intensities, i.e., distributions per analyzed cell without mAbs (A) and with mAbs for 0, 1, 2, 4, and 24 h of incubation at 37°C (B-F). There is only a slight overlap between the fluorescence distributions (see dot-plots A and B), indicating that BR96 has bound to nearly all cells at 0 h of incubation. These data also show that there is no significant contribution of nonspecific florescence signals.

At 1 h of incubation at 37°C (Fig. 1C, Table 1), a subpopulation (R2) comprising BR96-FITC positive cells was clearly separated from the main anti-IgG PE intensity distribution, comprising about 15% with small variations between the experiments (±2%). This separate population was indicated to represent BR96-LeY complexes that had been internalized into the cells, and the temporal pattern was further analyzed. The temporal analysis revealed the degree of putative cellular internalization by BR96 after 0, 1, 2, 4 and 24 h incubation, represented as the mean normalized ratio of FITC and PE fluorescence intensities (Table 1). The proportion of a putatively internalized BR96-FITC and nonanti-IgG-PE population increased after 1-2 h, whereas a slight decrease was noted between 2 and 4 h. However, the declination lies within 1 SD of the value at 2 h and is thus not statistically significant.

Table 1. Values for the Main Population (R1) and the Subpopulation (R2) of FITC and PE Fluorescent Cells Detected with FCM at the Different Incubation Times Illustrated In Figure 1

Time (h)	Main population, R1 (%)	Subpopulation, R2 (%)	Normalized ratio (FITC/PE)	Standard deviation
0	99	1	1	0
1	87	13	1.61	0.31
2	91	9	1.87	0.29
4	95	5	1.60	0.33
24	99	1	1	0

The mean normalized value of the ratio of FITC/PE fluorescence intensities after 0, 1, 2, and 4 and 24 h of incubation at 37°C with BR96-FITC followed by incubation with anti-IgG streptavidin-PE is also demonstrated.

Visualization - Microscopy Data

After short-term incubation with BR96-FITC (0 h at 37°C), wide-field epi-fluorescence microscopy demonstrated that BR96-FITC and IgG-PE or -TR fluorescence were located together, apparently at the cellular surface. The double labeling was more or less homogenously distributed throughout the whole cell population of each slide, depicted by coinciding BR96-FITC labeling and PI labeled nuclei. Following 1 h of incubation, the BR96-FITC fluorescence was relatively stronger, with an indicated intracellular localization, while the fluorescence colocalization with PE or TR was less obvious. No signal intensities comparable with the flourophore fluorescence signals were detected in control cells, i.e., in cells that had not been incubated with the primary antibodies, neither by wide field epi-fluorescence nor CLSM, which further supported a specific in vitro binding of BR96-FITC to LeY of the paraformaldehyde fixated H1D2 cells. The weak auto-fluorescence recorded in all channels (or filter combinations) was used as background signal level that was adjusted for in the CLSM analyses.

CLSM analyses confirmed that BR96-FITC was localized to the plasma cell membrane at 0 h and demonstrated that BR96-FITC was colocalized with IgG-TR at this location (Fig. 2A). From 1 h of incubation CLSM further revealed that strongly labeled BR96 was indeed localized within the cells, whereas less anti-IgG-TR labeling was present in the cell plasma membrane (Fig. 2B). Within the cytoplasm, internalized BR96-FITC/LeY was visualized as widespread and scattered small fluorescence signals in the cytoplasm and as aggregates of BR96 fluorescence labeling of varying sizes.
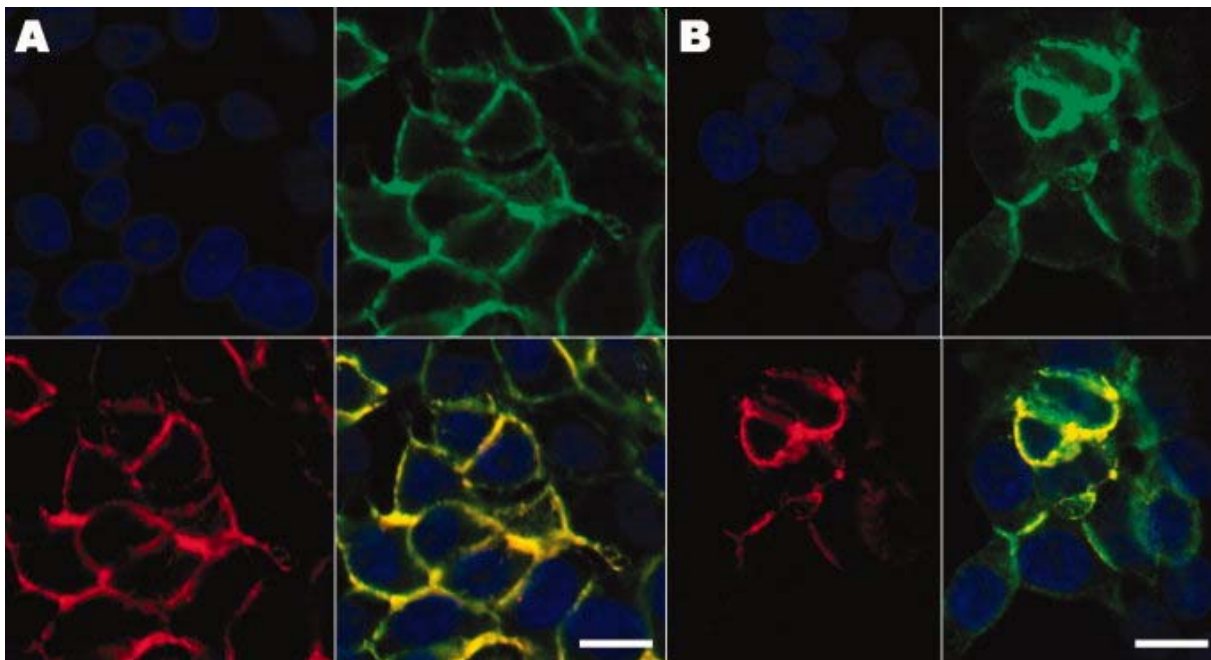
Figure 2.
Low magnification CLSM images of H1D2 cell populations (blue nuclear labeling) at 0 h (A) and 1 h (B) after incubation with BR96-FITC (at 37°C), demonstrating BR96-FITC (green) bound to LeY and anti-human IgG-streptavidin-TR bound to BR96 (red). Initially both BR96-FITC and IgG-streptavidin-TR are restricted to the cell plasma membrane (at 0 h), depicted by colocalized BR96-FITC and IgG-streptavidin-TR (yellow in merged images). One hour after incubation BR96-FITC is localized also inside the cells, together with anti-human IgG-streptavidin-TR, demonstrating that BR96-FITC/LeY complexes have started to internalize into the H1D2 cells. Scale bars represent 5µl for all images.

Following 2 h incubation (Fig. 3), relatively large BR96-FITC/LeY fluorescence aggregates had formed in a subpopulation of the cells. High intensities of BR96-FITC/LeY fluorescence was detected in the plasma cell membrane (Fig. 3A). At this time, BR96-FITC/LeY aggregates were detected in close association with the cell nucleus of some cells, and in some cases the aggregates were localized adjacent to, or in direct contact with, the nuclear membrane (Fig. 3B). Still, the largest amount of cells possessed also BR96-FITC/LeY signals that were distributed throughout most parts of the cytoplasm, depicted by varying sizes of aggregates (Figs. 3B and 3C). From 2 h incubation time the anti-IgG-TR fluorescence decreased significantly, or was not detected. From 1 hour incubation, several BR96-positive cells exhibited a cell nucleus with a morphologically pyknotic appearance, and the majority of cells with internalized BR96 were also TUNEL positive (Fig. 4).
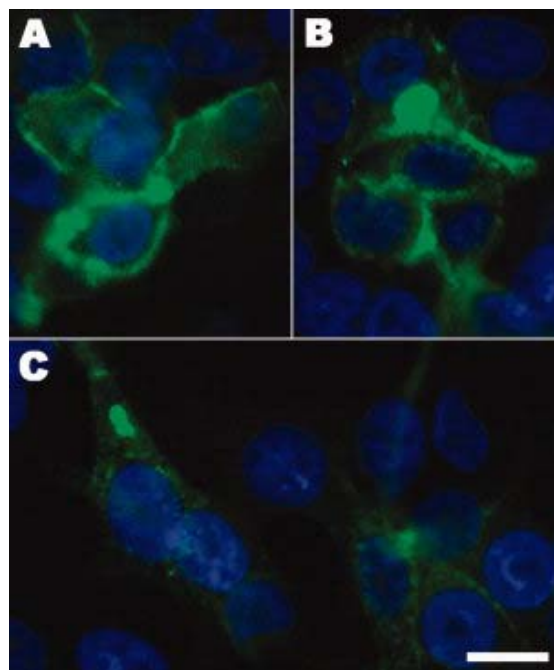
Figure 3.
CLSM images of H1D2 cells (blue nuclei in A, B, and C) after 2 h incubation with BR96-FITC (at 37°C) and labeled with anti-human IgG (red, streptavidin-TR). BR96-FITC (yellowish-green) bound to LeY is localized at the cell plasma membrane (preferentially in A); however, it is to a large degree distributed also within the cells, depicted by the different size BR96-FITC aggregates (or clusters) located in the cytoplasm (B and C). In some cells, BR96-FITC aggregates were closely associated with the cell nuclei (B). Note also that BR96 (streptavidin-TR, red or yellow when colocalized with BR96-FITC) is not visualized in the plasma membrane, which may indicate a high rate of internalization of BR96-FITC/LeY complexes. Scale bar in C represents 5 µm in A, B, and C.
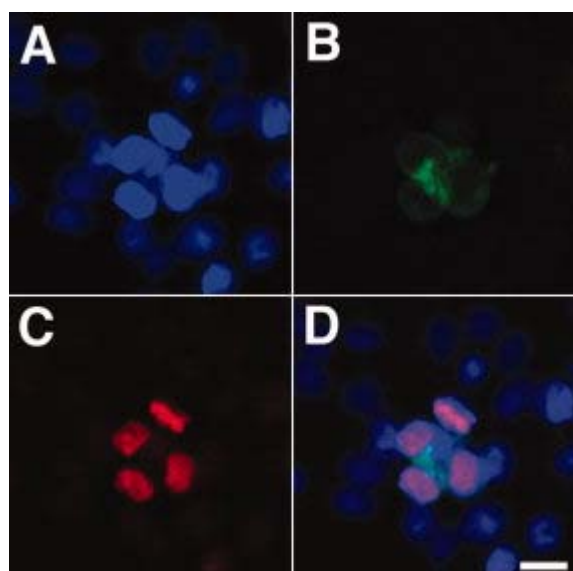
Figure 4.
CLSM images of a H1D2 cell population (blue nuclei, A) with BR96-FITC labeled (green, B) and TUNEL TR labeled (red, C) cells, 1 h after incubation at 37°C with BR96-FITC. The cytotoxic effects by BR96-FITC on H1D2 cells were supported by visualization of cells with bound BR96-FITC and TUNEL TR positive nuclei (D, cells with green labeling and purple nuclei). Scale bar in D represents 5 m in A, B, C, and D.

DISCUSSION

With the use of triple labeling techniques for combined FCM and CLSM analyses, we demonstrated the specific binding of BR96 to LeY in the cell plasma membrane of BN7005-H1D2 tumor cells, the heterogeneity of binding within the tumor cell population, and the capacity for BR96 to enter the cytoplasm of cancer cells (see combined data in Fig. 5). We describe the spatial-temporal internalization processes of BR96/LeY complexes and provide evidence for toxic effect by BR96 binding and/or internalization. In general, these comply with previous data from experimental studies on BR96 obtained by different techniques ([9][10][19]). The evaluated combined use of FCM and CLSM techniques for detection of the same or corresponding fluorescence labeled molecules is emphasized to provide a reliable tool in the optimization and development of mAb-complex targeting for different cancer cell types, with respect to both single cells and whole tumors.
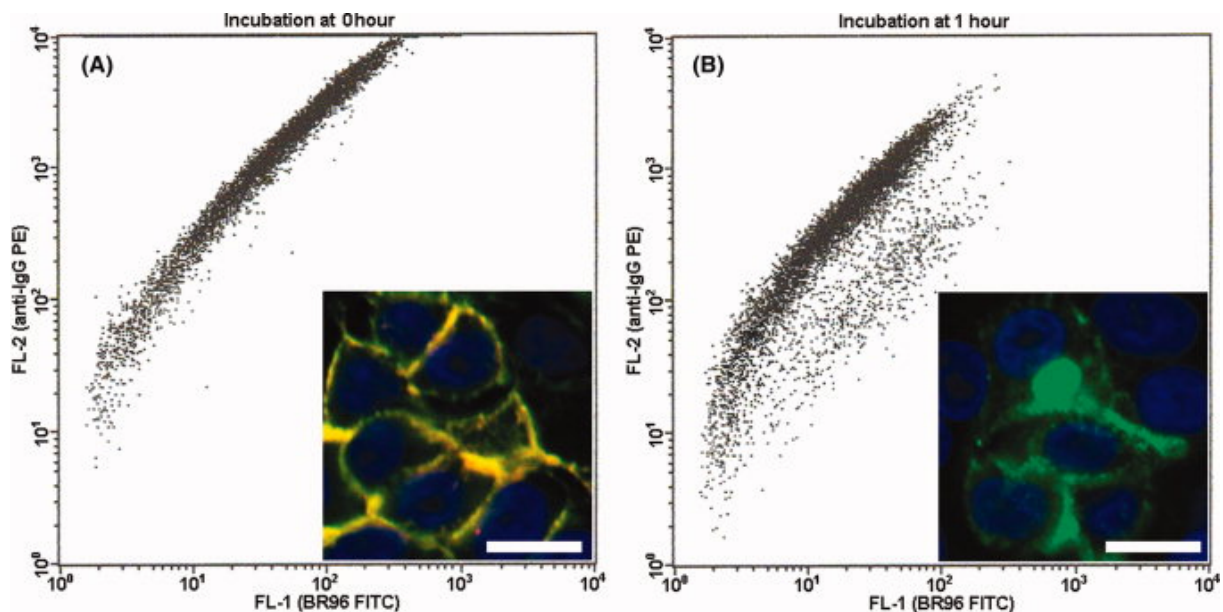
Figure 5.
Combined FCM dot plot graphs and CLSM images of BR96-FITC and IgG-PE after BR96-FITC incubation, at 0 h (A) and 1 h (B, see also Fig. 1C and Figs. 2 and 3). The representation demonstrates the quantitative data obtained in FCM as dot plots, which were directly correlated with the actual localization of BR96 visualized with CLSM, here shown localized to the cell plasma membrane (A) and within the cytoplasm of the distinct subpopulation (B). Scale bar represents 5 µm.

The cancer cell line BN7005-H1D2 used as target for BR96 in this study is of epithelial origin and has been characterized previously ([19][26][27]). Because of the epithelial origin, attachment to a surface by cell-to-cell adhesion is necessary for its cell function and subsequent survival. BR96-FITC was thus bound to the cells prior to cell detachment using trypsin. Correspondingly, in control experiment, comparing the internalization before and after trypsin treatment showed that neither BR96-FITC nor anti-IgG-PE fluorescence intensities were affected by trypsination (data not shown). The internalization process over the plasma cell membrane may not take place when in suspension. To prevent aggregation of the H1D2 cells after trypsination, the EDTA treatment and "mechanical" separation of cells (by pipetting of the cell suspension) provided mainly single and doublet formation of the cells (as verified by Bürker chamber microscopy and FCM light scatter dot-plots, data not shown).

Cell cycle analysis of H1D2 cells showed that there was a large fraction of cells in the S (48%) and G_2M (17%) phases, indicating that the cells are in the exponential growth phase and that they have a high proliferation rate. The calculated cell proliferation rates (from cell counting in Bürker chamber microscopy) indicated that the population doubling time is 12 h.

The doubling time for the H1D2 cell line is relatively short, which is why direct comparisons of temporal events with cell-lines with much lower cell cycle rates cannot be made. In future studies of BR96 internalization properties in human cancer cells, cell lines such as L56Br-C1 ([32]) and JIMT-1 ([33]) (established from two human primary breast cancers) should be investigated, which features cell cycle and cell kinetic data corresponding to the conditions in most human tumors. H1D2 cells have the unique ability to form primary tumors in immunocompetent rats ([19]). This model can contribute with important data about effects by BR96 treatment on whole tumors in vivo ([19][26][27]). Internalization was shown to be temperature dependent; that is, no internalization was seen at 4°C (on ice), which is consistent with previous findings ([9]). This temperature dependency thus indicates that the process of internalization is an active and energy-consuming process.

The mean intensity of both BR96-FITC and anti-IgG-PE fluorescence of all cell populations decreased with time, including a decrease in signal of the BR96-FITC subpopulation (from 13% to 1% in 24 h, Figs. 1D-1F, Table 1). The decrease in signal of the main population may represent general fading of the fluorophores, observed also in nonincubated cells. This may be due to loss of BR96-FITC binding and/or capping, whereas the decrease in signal of the putative internalized populations may also include degradation of BR96-FITC in the lysosomes ([3][10]).

This study showed that cell targeting and internalization of the mAb BR96 conjugated with FITC could be directly analyzed with FCM and CLSM. In previous studies, the FITC conjugate has been used as a target for immunolabeling with antibodies against FITC (anti-FITC) ([21]). Here, we combined the detection and visualization of BR96-FITC with detection of human IgG, detected and visualized via indirect labeling using a secondary mAb (anti human IgG) conjugated with biotin with streptavidin-PE or -TR. The degree of internalization was demonstrated with both FCM and CLSM based on the difference between mAb anti-IgG conjugated with biotin bound and with streptavidin-PE or -TR, and the BR96-FITC. This due to the fact that the anti-IgG antibody binds only to its antigens (here BR96) on the cellular surface, whereas the BR96 within the cell is not bound. Therefore, comparison of the flow cytometric fluorescence intensities of cells internalizing mAbs initially, and after a certain time, gives information on the degree of internalization (see Table 1). Compared with SDS page, western blotting, and visualization methods ([19][20]), this strategy for FCM analyses provided relatively rapid analysis of cellular bound and internalized antibodies in a large number of individual cells. The statistical values for the events of internalization presented here is solely from FCM analyses and the complement of CLSM visualization of the same or corresponding markers provided verification of the processes at the cellular level. Optimization of the method should be made related to the individual cell lines and/or mAbs investigated, including method sensitivity, specificity, and reproducibility.

Both FCM and CLSM identified the main populations and subpopulations representing binding and internalization by BR96 (see Fig. 5). The FCM analyses demonstrated that about 15% of the cells had heavy BR96/LeY internalization, a percentage supported by the appreciated number visualized with CLSM (data not shown). This subpopulation showed a relatively high degree of internalization, with a maximum degree of internalization after 1-2 h of incubation. Thereafter, the size of this population decreases and at 24 h it had disappeared. The mean normalized values show an increase in internalization during the first 1-2 h (Table 1). After that, a slight (but not statistically significant) decrease was noted (remaining up to 4 h), because internalized BR96/LeY is degraded in the lysosomes ([3][10]). For clinical therapy, a high internalization capacity of mAbs is critical when conjugated with toxins or short-range-particle-emitting radionuclides and may require that all or most subpopulations of cancer cells receive cellular internalization of the drug. Differently, high-energy-particle-

emitting radionuclides (90Y) with a longer range could be administered or coadministered in more heterogeneous tumors. Internalization of the mAbs can be a disadvantage when using labeling techniques for halogens such as ^{125}I, ^{131}I, and [211]At, since dehalogenation can lead to a loss of radionuclides from the tumor cells. Such losses may be overcome by the use of radiometals such as ^{111}In, ^{90}Y, or ^{177}Lu for mAb conjugation ([7][8][34-36]).

Both CLSM and FCM analyses indicated that cellular damage was caused by BR96 binding and/or BR96/LeY cellular internalization, corresponding to the cellular toxicity by BR96 reported in previous studies ([9][10]). CLSM showed that especially cells with internalized BR96-FITC in several cases possess pyknotic cell nuclei and/or were TUNEL positive, thus indicating cell death or early stage of apoptosis. FCM demonstrated that fragmentation of cell material appeared in the forward- and side-scatter dot-plots when H1D2 cells were bound by BR96, identified as a cluster with lower scatter signals compared with those from the unbound cells (data not shown). FCM cell cycle analysis of internalized BR96-FITC indicated an increase in the degradation of DNA material; however, the expected pre-G_0/G_1 peak could not be resolved due to considerable debris.

CONCLUSIONS

The FCM and CLSM techniques used for detection of the same or corresponding fluorescence labeled molecules allowed a rapid and direct correlation of quantitative and qualitative analyses of the same BR96-FITC incubated BN7005-H1D2 cell populations, i.e., statistically reliable FCM data collected from large quantities of cells confirmed with the CLSM visualization in situ at the cellular level of the cellular and intracellular localization from representative cell populations. FCM and CLSM used together demonstrated the spatial-temporal properties of BR96 to specifically bind to LeY in the cell plasma membrane of BN7005-H1D2 tumor cells and revealed the capacity for the BR96/LeY complex to enter the cytoplasm of identified cellular subpopulations. Furthermore, the degree and heterogeneity of internalization to subpopulations comprising around 15% of the total cells were demonstrated, calling for further optimization of the mAb internalization processes. The study also added evidence for the toxic effect of targeted cells by cellular internalization of BR96 which, together with the use in cancer treatment already demonstrated ([13-16]), emphasize that BR96 possesses the desirable properties for further optimization and use in cancer therapy, including as a carrier of cytotoxic agents.

It can be concluded that the combined use of FCM and CLSM can serve as a valuable tool for future optimization of BR96-cytotoxic complex in cancer therapy and for evaluations of new developed mAbs in targeting of different cancer cell types. To enhance the therapeutic effects by mAbs, future evaluations of the use of mAbs in different types of human cancer cell lines should engage improvements of specificity and accelerations of the internalization rate, and evaluations of their suitable conjugation with toxins or low-energy-particle-emitting radionuclides should be directed towards both single cells and whole tumors.

REFERENCES

1   Sharkey RM,Goldenberg DM. Targeted therapy of cancer: New prospects for antibodies and immunoconjugates (review). CA Cancer J Clin 2006; 56: 226-243.

2   Baldwin RW,Embleton MJ,Price MR. Monoclonal antibody-defined antigens on tumor cells. Biomembranes 1983; 11: 285-312.

3   Walker MA,King HD,Dalterio RA,Trail P,Firestone R,Dubowchik GM. Monoclonal antibody mediated intracellular targeting of tallysomycin S(10b). Bioorg Med Chem Lett 2004; 14: 4323-4327.

4   Lambert JM. Drug-conjugated monoclonal antibodies for the treatment of cancer (review). Curr Opin Pharmacol 2005; 5: 543-549.

5   Leone G,Sica S,Voso MT,Rutella S,Pagano L Treatment of acute leukaemias with monoclonal antibodies: current status and future prospects (review). Cardiovasc Hematol Agents Med Chem. 2006; 4: 33-52.

6   Abutalib SA,Tallman MS. Monoclonal antibodies for the treatment of Acute myeloid leukemia. Curr Pharm Biotechnol 2006; 7: 343-369.

7   Brans B,Linden O,Giammarile F,Tennvall J,Punt C. Clinical applications of newer radionuclide therapies (review). Eur J Cancer 2006; 42: 994-1003.

8   Lindén O,Hindorf C,Cavallin-Ståhl E,Wegener WA,Goldenberg DM,Horne H,Ohlsson T,Stenberg L,Strand SE,Tennvall J. Dose-fractionated radioimmunotherapy in non-Hodgkin's lymphoma using DOTA-conjugated, 90Y-radiolabeled humanized anti-CD22 monoclonal antibody, epratuzumab. Clin Cancer Res 2005; 11: 5215-5222.

9   Hellstrom I,Garrigues HJ,Garrigues U,Hellstrom KE. Highly tumor-reactive, internalizing, mouse monoclonal antibodies to Le(y)-related cell surface antigens. Cancer Res 1990; 50: 2183-2190.

10   Garrigues J,Garrigues U,Hellstrom I,Hellstrom KE. Ley specific antibody with potent anti-tumor activity is internalized and degraded in lysosomes. Am J Pathol 1993; 142: 607-622.

11   Chen BX,Erlanger BF. Intracellular delivery of monoclonal antibodies. Immunol Lett 2002; 84: 63-67.

12   Siegall CB,Chace D,Mixan B,Garrigues U,Wan H,Paul L,Wolff E,Hellstrom I,Hellstrom KE. In vitro and in vivo characterization of BR96 sFv-PE40. A single-chain immunotoxin fusion protein that cures human breast carcinoma xenografts in athymic mice and rats. J Immunol 1994; 152: 2377-2384.

13   Henry CJ,Buss MS,Hellstrom I,Hellstrom KE,Brewer WG,Bryan JN,Siegall CB. Clinical evaluation of BR96 sFv-PE40 immunotoxin therapy in canine models of spontaneously occurring invasive carcinoma. Clin Cancer Res 2005; 11(2 Pt 1): 751-755.

14   Saleh MN,Sugarman S,Murray J,Ostroff JB,Healey D,Jones D,Daniel CR,LeBherz D,Brewer H,Onetto N,LoBuglio AF. Phase I trial of the anti-Lewis Y drug immunoconjugate BR96-doxorubicin in patients with Lewis Y-expressing epithelial tumors. J Clin Oncol 2000; 18: 2282-2292.

15   Posey JA,Khazaeli MB,Bookman MA,Nowrouzi A,Grizzle WE,Thornton J,Carey DE,Lorenz JM,Sing AP,Siegall CB,LoBuglio AF,Saleh MN. A phase I trial of the single-chain immunotoxin SGN-10 (BR96 sFv-PE40) in patients with advanced solid tumors. Clin Cancer Res 2002; 8: 3092-3099.

16   Tolcher AW,Sugarman S,Gelmon KA,Cohen R,Saleh M,Isaacs C,Young L,Healey D,Onetto N,Slichenmyer W. Randomized phase II study of BR96-doxorubicin conjugate in patients with metastatic breast cancer. J Clin Oncol 1999; 17: 478-484.

17   Sakamoto J,Yin BW,Lloyd KO. Analysis of the expression of H, Lewis, X, Y and precursor blood group determinants in saliva and red cells using a panel of mouse monoclonal antibodies. Mol Immunol 1984; 21: 1093-1098.

18   Ramsland PA,Farrugia W,Bradford TM,Mark Hogarth P,Scott AM. Structural convergence of antibody binding of carbohydrate determinants in Lewis Y tumor antigens. J Mol Biol 2004; 340: 809-818.

19   Sjogren HO,Isaksson M,Willner D,Hellstrom I,Hellstrom KE. Trail PAs antitumor activity of carcinoma-reactive BR96-doxorubicin conjugate against human carcinomas in athymic mice and rats and syngeneic rat carcinomas in immunocompetent rats. Cancer Res 1997; 57: 4530-4536.

20   Matzku S,Brocker EB,Bruggen J,Dippold WG,Tilgen W. Modes of binding and internalization of monoclonal antibodies to human melanoma cell lines. Cancer Res 1986; 46: 3848-3854.

21   Ford CH,Tsaltas GC,Osborne PA,Addetia K. Novel flow cytometric analysis of the progress and route of internalization of a monoclonal anti-carcinoembryonic antigen (CEA) antibody. Cytometry 1996; 23: 228-240.

22   Austin CD,De Maziere AM,Pisacane PI,van Dijk SM,Eigenbrot C,Sliwkowski MX,Klumperman J,Scheller RH. Endocytosis and sorting of ErbB2 and the site of action of cancer therapeutics trastuzumab and geldanamycin. Mol Biol Cell 2004; 15: 5268-5282.

23   Austin CD,Wen X,Gazzard L,Nelson C,Scheller RH,Scales SJ. Oxidizing potential of endosomes and lysosomes limits intracellular cleavage of disulfide-based antibody-drug conjugates. Proc Natl Acad Sci USA 2005; 102: 17987-17992.

24   Zucker RM. Quality assessment of confocal microscopy slide based systems: performance. Cytometry A 2006; 69A: 659-676.

25   Stephen D. Cell Imaging (Methods Express Series). Kent, UK: Scion; 2006.

26   Hegardt P,Widegren B,Li L,Sjogren B,Kjellman C,Sur I,Sjogren HO. Nitric oxide synthase inhibitor and IL-18 enhance the anti-tumor immune response of rats carrying an intrahepatic colon carcinoma. Cancer Immunol Immunother 2001; 50: 491-501.

27   Garkavij M,Tennvall J,Strand SE,Sjogren HO,JianQing C,Nilsson R,Isaksson M. Extracorporeal whole-blood immunoadsorption enhances radioimmunotargeting of iodine-125-labeled BR96-biotin monoclonal antibody. J Nucl Med 1997; 38: 895-901.

28   Zelenin AV,Poletaev AI,Stepanova NG,Barsky VE,Kolesnikov VA,Nikitin SM,Zhuze AL,Gnutchev NV. 7-Amino-actinomycin D as a specific fluorophore for DNA content analysis by laser flow cytometry. Cytometry 1984; 5: 348-354.

29   Baldetorp B,Dalberg M,Holst U,Lindgren G. Statistical evaluation of cell kinetic data from DNA flow cytometry (FCM) by the EM algorithm. Cytometry 1989; 10: 695-705.

30   Baldetorp B,Ferno M,Fallenius A,Fallenius-Vecchi G,Idvall I,Olsson H,Sigurdsson H,Akerman M,Killander D. Image cytometric DNA analysis in human breast cancer analysis may add prognostic information in diploid cases with low S-phase fraction by flow cytometry. Cytometry 1992; 13: 577-585.

31   Vindelov LL,Christensen IJ,Nissen NI. Standardization of high-resolution flow cytometric DNA analysis by the simultaneous use of chicken and trout red blood cells as internal reference standards. Cytometry 1983; 3: 328-331.

32   Johannsson OT,Staff S,Vallon-Christersson J,Kytola S,Gudjonsson T,Rennstam K,Hedenfalk IA,Adeyinka A,Kjellen E,Wennerberg J,Baldetorp B,Petersen OW,Olsson H,Oredsson S,Isola J,Borg A. Characterization of a novel breast carcinoma xenograft and cell line derived from a BRCA1 germ-line mutation carrier. Lab Invest 2003; 83: 387-396.

33   Tanner M,Kapanen AI,Junttila T,Raheem O,Grenman S,Elo J,Elenius K,Isola J. Characterization of a novel cell line established from a patient with Herceptin-resistant breast cancer. Mol Cancer Ther 2004; 3: 1585-1592.

34   Martensson L,Wang Z,Nilsson R,Ohlsson T,Senter P,Sjogren HO,Strand SE,Tennvall J. Determining maximal tolerable dose of the monoclonal antibody BR96 labeled with 90Y or 177Lu in rats: Establishment of a syngeneic tumor model to evaluate means to improve radioimmunotherapy. Clin Cancer Res 2005; 11(19 Pt 2): 7104s-7108s.

35   Wang Z,Martensson L,Nilsson R,Bendahl PO,Lindgren L,Ohlsson T,Sjogren HO,Strand SE,Tennvall J. Blood pharmacokinetics of various monoclonal antibodies labeled with a new trifunctional chelating reagent for simultaneous conjugation with 1,4,7,10-tetraazacyclododecane-N,N,N,N-tetraacetic acid and biotin before radiolabeling. Clin Cancer Res 2005; 11(19 Pt 2): 7171s-7177s.

36   Sharkey RM,Behr TM,Mattes MJ,Stein R,Griffiths GL,Shih LB,Hansen HJ,Blumenthal RD,Dunn RM,Juweid ME,Goldenberg DM. Advantage of residualizing radiolabels for an internalizing antibody against the B-cell lymphoma antigen, CD22. Cancer Immunol Immunother 1997; 44: 179-188.